Available online at www.sciencedirect.com

SciVerse ScienceDirect

www.elsevier.com/locate/matchar

High temperature fatigue crack growth of Haynes 230

Garrett J. Pataky[a], *Huseyin Sehitoglu*[a,*], *Hans J. Maier*[b]

[a]*Department of Mechanical Science and Engineering, University of Illinois at Urbana-Champaign, 1206 W. Green St., Urbana, IL 61801, USA*
[b]*Lehrstuhl für Werkstoffkunde (Materials Science), University of Paderborn, 33095 Paderborn, Germany*

ARTICLE DATA

Article history:
Received 5 July 2012
Received in revised form
25 September 2012
Accepted 29 September 2012

Keywords:
Fatigue crack growth
Digital image correlation
Nickel-based superalloy
Crack closure
Slip irreversibility

ABSTRACT

The fatigue crack growth of the nickel-based superalloy Haynes 230 was investigated at room temperature and 900 °C using digital image correlation (DIC). As expected, the crack growth rates at high temperature were much faster than at room temperature. However, the crack closure levels, which were determined using digital image correlation analysis techniques, were found to be similar for the two cases studied. DIC strain fields and the corresponding plastic zone sizes were compared between the two cases. From these strain fields, the slip irreversibility, the difference between forward and reversed strains at the crack tip, was quantitatively measured. The high temperature case had an order of magnitude higher amount of slip irreversibility. Slip irreversibility measurements were determined to be an effective method to compare fatigue crack growth of cases with differing temperatures.

1. Introduction

With the worldwide demand for energy rapidly accelerating, sustainable energy is imperative to economic development. One solution is to accelerate integration of next generation energy systems such as very high temperature reactors (VHTR). The VHTR requires elevated temperatures, up to 1000 °C, to boost efficiency [1]. These conditions are extremely demanding on the materials and are within a regime where our understanding of degradation processes is limited. This research will focus on the high temperature fatigue crack growth of the nickel-based superalloy Haynes 230.

Fatigue crack growth is extremely detrimental to the life of engineering components and has been the focal point of much research. Traditionally, there have been two distinct areas of concern when studying fatigue cracks: the crack wake and the crack tip. Crack closure is a phenomenon which occurs in the wake of the fatigue crack and has been used to describe the reduction of load seen by a crack during a fatigue loading cycle [2]. Plasticity-induced crack closure is shown in Fig. 1. A variety of methods to measure the level of crack closure have been employed historically including displacement gages, lasers, and potential drop measurements [3]. The advent of digital image correlation (DIC) provided a method to assess crack closure locally at the crack tip using digital (virtual) extensometers and globally using full field displacements [4–6]. The reduction of the stress intensity factor range due to crack closure provides a more general relationship to describe crack growth rates by removing the influence of loading factors such as the load ratio, R [7]. Although this modification has been very beneficial to describing fatigue crack growth behavior, it does not provide a complete explanation to crack growth rate variations. Alternatively, other studies of fatigue crack growth have focused on the fatigue crack tip, the plastic zone, and the dislocation interactions with the microstructure.

Models which describe fatigue crack growth rates as a crack tip phenomenon have been continually refined to smaller scales as new developments were made. Tomkins was the first to relate crack tip plasticity to the crack growth rate using Dugdale's plastic cohesive stress model [8]. During the unloading portion of a fatigue cycle, reverse plasticity occurs due to the reversal of

* *Corresponding author.*
E-mail address: huseyin@illinois.edu (H. Sehitoglu).

1044-5803/$ – see front matter © 2012 Elsevier Inc. All rights reserved.
http://dx.doi.org/10.1016/j.matchar.2012.09.012

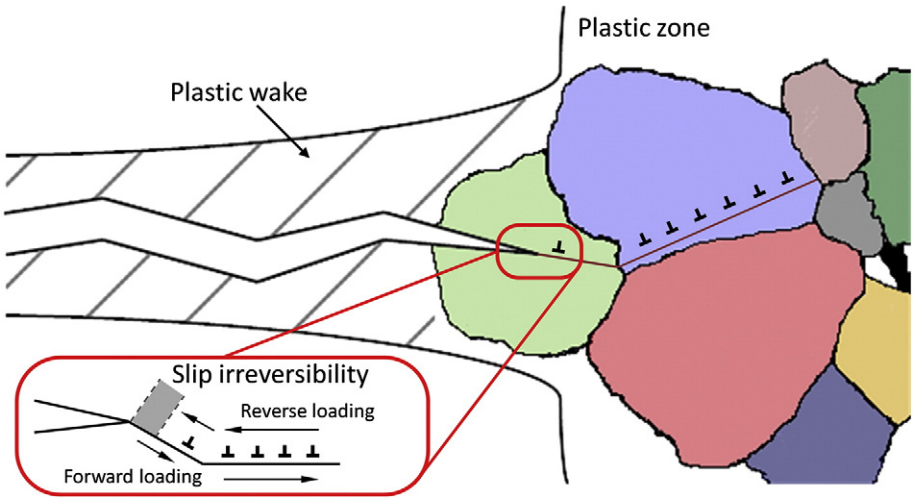

Fig. 1 – A schematic of a fatigue crack with plasticity-induced crack closure in the crack wake and slip irreversibility at the crack tip. The shaded grey region in the inset provides a measure of the irreversible slip strain (or irreversible displacements).

loading. This creates a reversed (or cyclic) plastic zone ahead of the crack tip within the monotonic plastic zone [9,10]. Further works relating the fatigue crack growth rate to plastic zones relied on using this ideology of a reversed plastic zone [11,12]. It was determined that a larger reversed plastic zone size would cause an increase in the fatigue crack growth rate. Using a finite element analysis, McClung and Sehitoglu were able to demonstrate that crack closure can affect the reversed plastic zone size [13].

With evolution of crack tip plasticity being the major driving force in fatigue crack growth in ductile materials, light had to be shed on the role played by dislocations. Early discoveries included the finding that cross slip had a direct influence on the rate of crack propagation [14]. Forsyth explored crack initiation and observed that as dislocations cross slipped, extrusions formed. As the cross slipping of dislocations occurred at the extruded material, a crack formed [15]. Building upon this observation, Fong and Tromans developed a model of restricted slip reversal to describe crack growth in terms of dislocations emitted from the crack tip during cyclic loading [16]. This concept introduced slip irreversibility and is shown in Fig. 1. Pippan studied the force required to emit dislocations at the crack tip and related the quantity of emitted dislocations that do not fully reverse to the crack growth rate [17,18]. Wu *et al.* related the plastic strain ahead of the crack tip, due to slip irreversibility, to the fatigue crack growth rate [19]. A technique using DIC has been developed to determine the quantity of residual crack tip plastic strain and has been demonstrated for several materials at room temperature [7,20].

The current study will provide further experimental insight into fatigue crack growth at elevated temperatures. Haynes 230 was studied due to its good corrosion resistance and properties at elevated temperatures making it a viable candidate for structures under extreme conditions. The analysis encompasses both the previously discussed phenomena of crack closure and of slip irreversibility. Using novel techniques to employ DIC at 900 °C, it will be shown that slip irreversibility at the crack tip is the key damage mechanism driving fatigue crack growth.

2. Materials and Experimental Procedure

2.1. *Materials*

The experiments in this study were performed on the commercially available nickel-based superalloy Haynes 230. The chemical composition for the sheet used is shown in Table 1. Haynes 230 is a solid-solution strengthened alloy, and the additions of chromium, tungsten, and molybdenum contribute to the high temperature properties of the alloy. The typical microstructure has a wide range of grain sizes and is displayed in the optical photomicrograph in Fig. 2. Using the linear intercept method, as outlined in ASTM E-112, the average grain size was found to be about 50 μm. A large amount of annealing twins was observed in the material, so electron back-scatter diffraction (EBSD) was performed on an area of approximately 0.39 mm^2 to obtain statistical information. A portion of the EBSD data is shown in Fig. 3a. Fig. 3b has a histogram of the coincident lattice notation, CSL, grain boundary types for the entire area scanned. 573 out of the 1249 grain boundaries were described using the CSL criterion and almost two-thirds were Σ3 boundaries.

The sheet received was 2.38 mm (3/32″) thick, and single-edge notch "dogbone" specimens were electrical discharge machined (EDM) with a gauge length of 25.00 mm and width of 4.00 mm.

Table 1 – Chemical composition (wt%) of Haynes 230 studied.

Al	B	C	Co	Cr	Cu	Fe	La	Mn
0.35	0.005	0.1	0.16	22.14	0.04	1.14	0.015	0.5
Mo	Ni	P	S	Si	Ti	W	Zr	
1.25	bal	0.005	0.002	0.49	0.01	14.25	0.01	

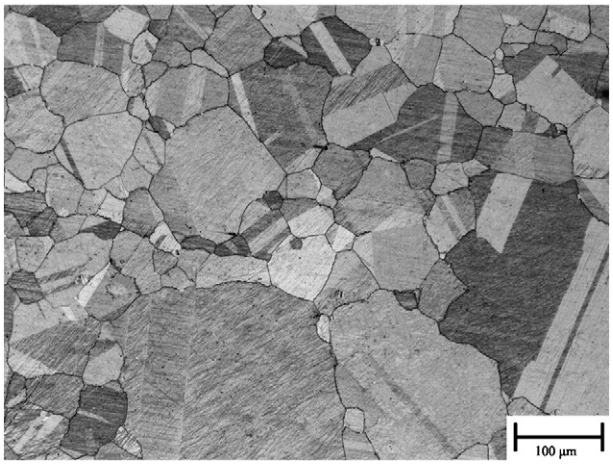

Fig. 2 – Microstructure of the as-received Haynes 230 material showing annealing twins and a wide range of grain sizes.

A 0.5 mm deep notch was EDM in the center of the gauge length to facilitate pre-cracking during the fatigue crack growth experiments.

2.2. *Experimental Procedure*

In order to prepare the specimens for DIC, two separate procedures were required depending on the temperature condition. For the room temperature (RT) experiment, the specimens were mechanically polished to a mirror finish using abrasive paper up to P2400 grit size. Black paint was then airbrushed onto the specimen surface to create a speckled pattern. The high temperature (HT) experiment required a different preparation since at 900 °C the sample glowed. The front of the sample was painted white with a thin layer of very high temperature paint. The paint was then cured using a three-step process, exposing it to a maximum temperature of 315 °C. A layer of black paint was then airbrushed onto the specimen as was done with the room temperature experiment. The white paint was required for the HT sample to reduce the brightness that comes with the glowing and to prevent the speckle pattern from changing due to oxidation.

A servo-hydraulic load frame was used during the experiments. The HT specimen was heated using induction heating. A type-K thermocouple was spot welded on the middle of the back of the specimen approximately 2 mm above the notch plane. While at zero load, the specimen was heated at a rate of 75 °C per minute until the sample reached 900 °C. The temperature was kept within ±3 °C for the entirety of the experiment. An IMI 202FT digital camera was used to capture images during the fatigue crack growth experiments. The camera resolution was 1600 pixels by 1200 pixels, the maximum frame rate was 15 fps, and an adjustable lens with a 12× magnification range and 2× adapter was used to achieve different magnifications. A magnification of 2.5× was used to capture the images. The specimens were loaded in fatigue at a load ratio, R, of 0.05 at a frequency of 3 Hz. The RT specimens were fatigue loaded with a stress range of 270 MPa. The stress range had to be reduced due to the lower yield stress at 900 °C, and the HT specimen was fatigue loaded with a stress range of 104.5 MPa. A computer program controlled the servo-hydraulic load frame and captured images and their corresponding loads measured by a 7.5 kN load cell during the test. Once a crack was visually identified, measurement cycles were periodically run at a frequency of 0.25 Hz in order to capture a greater number of images per cycle to provide an in-depth analysis into the fatigue cycles.

A commercially available image correlation program was used to perform DIC analysis. For a description of the digital image correlation technique, see [21,22]. For the crack closure analysis, the first image of each measurement cycle, captured at minimum load, was used as the reference image for that

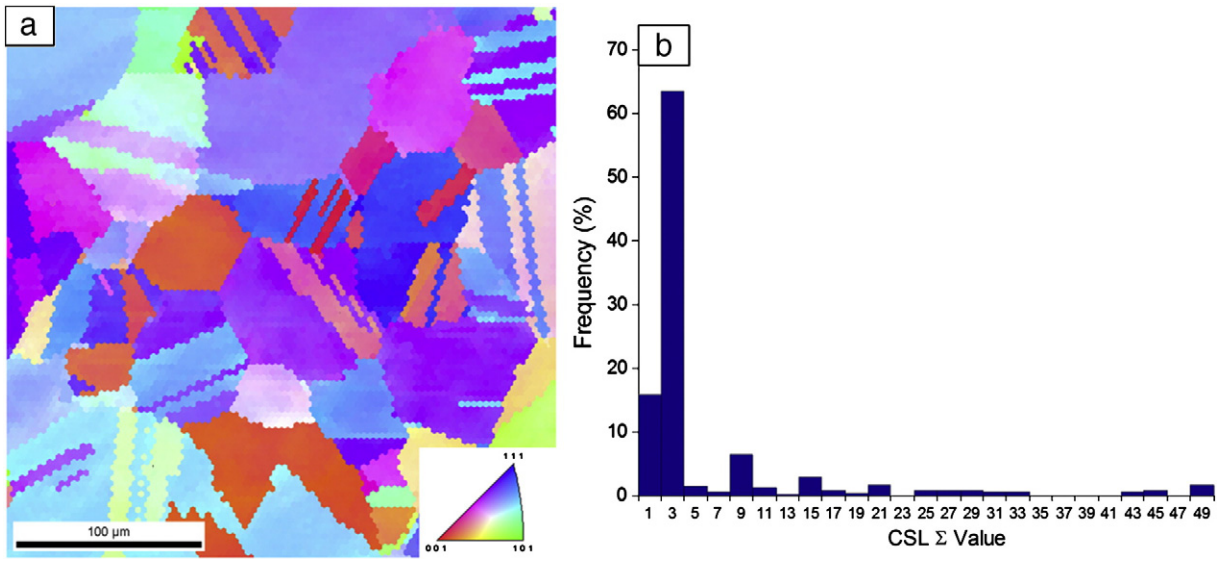

Fig. 3 – a) A section of the grain orientation map from EBSD of Haynes 230. b) The CSL boundary frequency for the 0.39 mm^2 area scanned showing a high percentage of ∑3 boundaries.

cycle. When studying slip irreversibility, the first image of the experiment, again captured at minimum load, was used as the reference image since strains due to the crack were not present yet. The full field of displacements, both behind and ahead of the crack tip, was used for correlations. The displacements were used in the least-squares regression, as briefly described in the Appendix, in order to determine the effective stress intensity factor ranges and crack closure levels. At each correlated point, the horizontal (x) and vertical (y) displacements were calculated and differentiated to obtain the strains assuming a small strain approximation.

For transmission electron microscopy (TEM) 1 mm thick discs were sectioned with a low-speed diamond saw parallel to the loading axis from the failed specimens, and then mechanically ground and polished down to 0.15 mm foil thickness. Large electron transparent areas were obtained in these foils by conventional twin jet polishing using a solution consisting of 5pct perchloric acid in ethanol at 20 °C and 15 V. The TEM was operated at a nominal voltage of 200 kV and a double-tilt specimen holder was employed for imaging under two-beam conditions.

3. Results

3.1. Tensile Tests

To determine the mechanical properties of Haynes 230 at both RT and HT (900 °C), a simple uniaxial tension test was performed at each temperature as shown in Fig. 4. Using DIC, the 0.2% offset yield stress was determined to be 415 MPa for the RT sample and 123 MPa for the HT sample. Another difference between the two stress–strain responses is the continual hardening in the RT experiment and the almost immediate softening in the HT experiment.

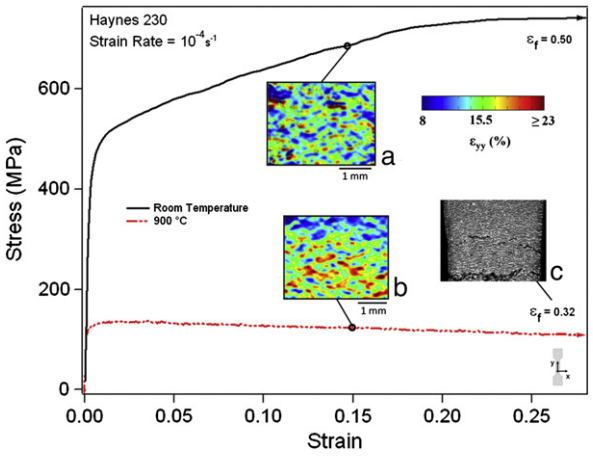

Fig. 4 – The stress–strain response of Haynes 230 at room temperature and 900 °C with fracture strains of 50% and 32% respectively. The DIC strain plots at 15% global strain show the greater localization at 900 °C.

Observing the DIC strain fields, labeled a) and b) in Fig. 4, for about 15% strain, the HT result shows far more localization than the RT result. The image of the HT specimen surface near fracture, labeled c), shows significant damage along the section that fails. Necking and large voids are observed in the entire area shown. The fracture strain of the two specimens is quite different and the lack of damage in the RT sample would be a reasonable explanation for this result.

3.2. Fatigue Crack Growth

Images were continuously taken during the fatigue crack growth tests to use digital image correlation to capture the full field displacements. Crack growth rates were determined by using these images to follow the crack tip advancement. As indicated in Fig. 5, both RT and HT fatigue crack growth tests were run. The solid symbols in Fig. 5 represent the isotropic stress intensity factor range calculation

$$K \quad {}^{p} \quad a\, f\, {}^{a}\!=_{w} \qquad 1$$

where Δ is the stress range, a is the current crack length, and $f\, {}^{a}\!=_{w}$ is the geometric correction factor which can be found in [23]. Eq. (1) does not account for crack closure though. The least-squares regression code explained in [4] and the Appendix was used to extract the effective stress intensity factor range from the experiments by considering the full field crack tip displacements which inherently are effected by crack closure during a fatigue cycle. The effective stress intensity factor results which consider crack closure are shown as hollow symbols in Fig. 5. The insets included in this figure show the experimental and regressed vertical displacement contours corresponding to

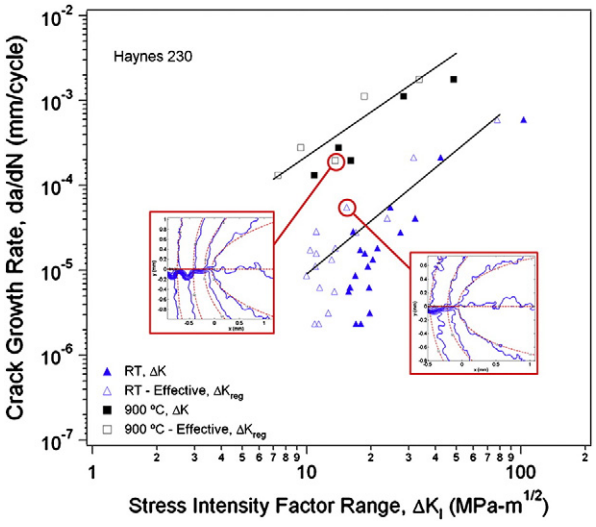

Fig. 5 – The crack growth rate as a function of the stress intensity factor range for room temperature (RT) and 900 °C experiments. The inserts are displacement contour plots showing the experimental (blue) and regression (red) vertical displacements in increments of 1 micron with the black dot indicating the crack tip location.

Table 2 – Paris law coefficients for Haynes 230 at RT and 900 °C (da/dN in mm/cycle and K in MPa√m).

	C	m
RT theoretical	1.34E-08	2.38
RT effective	7.54E-08	2.08
900 °C theoretical	1.81E-06	1.82
900 °C effective	4.20E-06	1.74

the RT and HT specimens. The Paris law coefficients and exponents for both tests are shown in Table 2. The Paris law exponent is about 2 for both test results which is in the common range of 2 to 4 for metals [24]. The following form of the Paris law was used to find the effective results which considered crack closure

$$\frac{da}{dN} \quad C \quad K_{eff}^{\ m} \qquad 2$$

where

$$K_{eff} \quad {}_{eff}^{\ p} \quad a\ f\ {}^{a}{}_{=w} \qquad 3$$

C and *m* are the Paris coefficient and exponent respectively, Δ_{eff} is the effective stress range (the portion of the loading cycle the crack is open), and *a* is the crack length.

The crack growth rate for the HT experiment was over an order of magnitude higher than in the RT experiment, being in the range of 10^{-3} to 10^{-2} mm/cycle. This is an extremely high rate of fatigue crack growth and could lead to failure in a component before the crack is initially detected. Comparing the isotropic and effective stress intensity factor values, the crack closure level for both experiments was an average of 30% of the load. To show the effectiveness of the regression technique in determining the closure level, two-point digital extensometers, which measure local crack opening levels, were used to find closure values along the crack length for both the RT and HT specimens. The comparison results are provided in Fig. 6. The regression technique, also referred to as the full-field method, proved to be efficient in mainly estimating the overall crack closure levels, while the two-point digital extensometers provided insight into the precise crack closure levels at the crack tip. The similarity in the closure levels between the two specimens is a surprising result and provides no conclusion about the faster crack growth rate at HT, thus, slip irreversibility was investigated.

3.3. *Slip Irreversibility*

With the stress intensity factors known, a plane stress assumption was used to approximate the plastic zone size [25]. Shown in Fig. 7a is the plastic zone for the RT specimen at crack length of 0.994 mm at maximum load. The blue contours represent the experimental displacement contours in micrometers, and the red contours are the displacement contours in micrometers found using the values from the least-squares regression. Using the effective stress intensity factor of 16.55 MPa m, the plastic zone radius was determined to be 0.337 mm. Strains found from digital image correlation were inserted into the plastic zone and high values of strain are found throughout the plastic zone. To compare, an

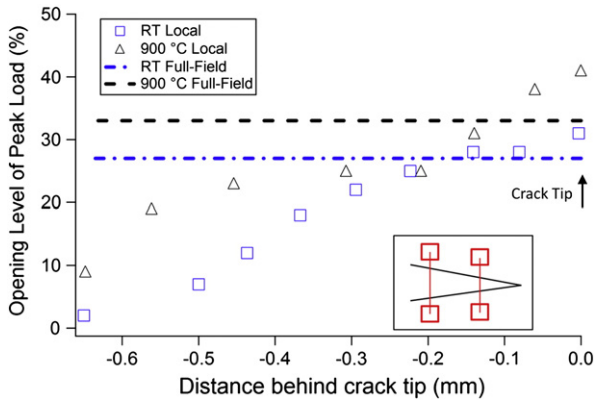

Fig. 6 – A comparison between the local (digital extensometer) and full-field (regression) crack opening levels for the RT specimen at a crack length of 0.994 mm and the HT specimen at a crack length of 0.964 mm. Symbols represent the digital extensometer values at various points along the crack while lines represent the regression found value for the full-field. The schematic depicts the digital extensometer technique and placement along the crack flanks.

HT specimen cycle at a crack length of 0.964 mm was used as shown in Fig. 7b. The effective stress intensity factor for this crack length was 9.39 MPa m and the corresponding plastic zone radius was found to be 0.664 mm. The strains in the plastic zone show a concentration around the crack tip. Even though the HT specimen had a much smaller effective stress intensity factor range, the lower yield stress caused the plastic zone size to be approximately twice that of the RT specimen at the same crack length.

Although these plastic zone approximations give much insight into the plasticity caused by the fatigue crack growth, the crack tip slip irreversibility was of great interest due to its correlation with the crack growth rate. As dislocations are emitted from the crack tip during a fatigue cycle and do not fully reverse to the crack tip, strain is accumulated. In order to capture this behavior, measurements of the strain were made at the beginning and end of the cycle. Thus, the difference between points A and B, shown in the bottom right of Fig. 8, can be considered the slip irreversibility for one cycle. To quantitatively measure this at the meso-scale, DIC has been utilized. The DIC strain plots in Fig. 8 are used as an example of this technique. The two strain plots are one cycle apart, with the image labeled "A" being recorded at the beginning of the cycle and the image labeled "B" being at the end. The isotropic and effective stress intensity factor ranges were 24.6 MPa m and 15.4 MPa m respectively with a crack closure level of 37% for the RT example and 13.86 MPa m and 9.39 MPa m respectively with a crack closure level of 32% for the HT example. The strain plots show strain at the crack tips before the cycle for point "A" (referring to Fig. 8) and then after the cycle for point "B" which shows residual strains at the crack tip. Taking advantage of the digital image correlation resolution, strain measurements in front of the crack at points "A" and "B" were compared and irreversible strains

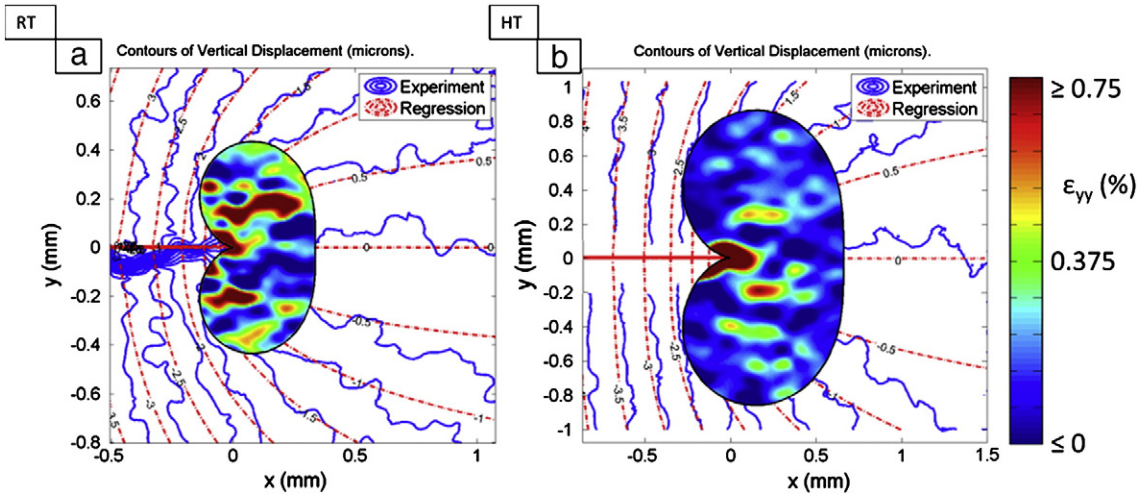

Fig. 7 – Plots of vertical displacement contours and plastic zones for a selected a) room temperature and b) 900 °C fatigue crack cycle. Blue contours represent the experimental DIC displacements and red contours represent the regression found displacement contours. a) At a crack length of 0.994 mm, the room temperature specimen had a K value of 22.64 MPa√m, a regression found K_{eff} value of 16.55 MPa√m, and a plastic zone radius of 0.337 mm. b) At a crack length 0.964 mm, the 900 °C specimen had a K value of 14.08 MPa√m, a regression found K_{eff} value of 9.39 MPa√m, and a plastic zone radius of 0.666 mm.

of 6.35×10^{-4} for the RT sample and 5.36×10^{-3} for the HT specimen were measured. This technique was applied for multiple crack lengths of the RT and HT specimens. As with the two examples provided, the trend of the HT specimen having irreversible strain an order of magnitude higher than the RT specimen was consistent throughout as shown in Fig. 8.

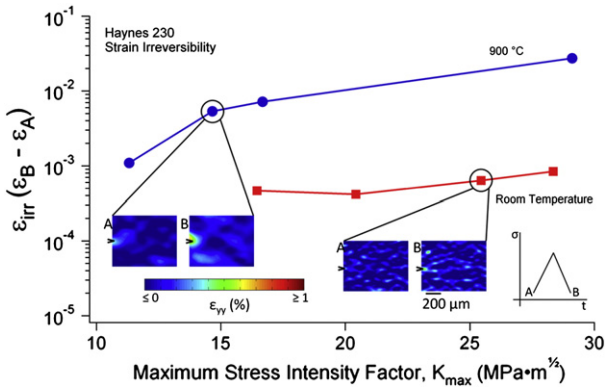

Fig. 8 – Strain irreversibility as a function of the maximum stress intensity factor during the fatigue crack growth experiments. The schematic shows the two minimum load points (A and B) where the strain measurements were taken. DIC strain plots for both the room temperature and 900 °C experiments are shown and the higher strains in the B plots compared to the A plots indicated irreversible strains during the fatigue cycle.

3.4. *Scanning Electron Microscope and Transmission Electron Microscopy Analysis*

In order to further understand the microstructural response of the Haynes 230 sample fatigued at 900 °C, images of the fracture surface were taken with a scanning electron microscope (SEM) and the dislocation arrangements were observed with transmission electron microscopy (TEM). The first SEM micrograph, shown in Fig. 9a, shows the classic striations attributed to cyclic fatigue crack growth. This verifies that the external loading was responsible for the propagation of the crack and ultimately the failure of the material. Also evident in this micrograph is the effects of the high temperature damage as it was taken in a region that experienced a high ΔK. Fig. 9b provides an example of the smoothness of the surface signifying the low amount of oxidation present. This is consistent with the Haynes International, Inc. data and previously completed research [26,27].

A TEM analysis was then performed to observe the dislocations and any other phenomena present. As shown in Fig. 10, planar slip was observed. This is consistent with other solid-solution hardened fcc alloys [28] and other nickel-based superalloys fatigued at high frequencies at high temperatures [29]. Also of particular interest was the formation of subgrains with several being present in the image. This was seen throughout the specimen with another example being given in Fig. 11. Obvious from this TEM image is a large heterogeneity in the microstructure. On the left, dislocations are present with nothing to impede their motion. Dividing the image in half is a stacking fault. On the right half of the image, intense dislocation–carbide interactions are observed providing for substantial resistance to dislocation motion. There are two types of carbides present in this image which are assumed to be M_6C and $M_{23}C_6$. The larger of the two found

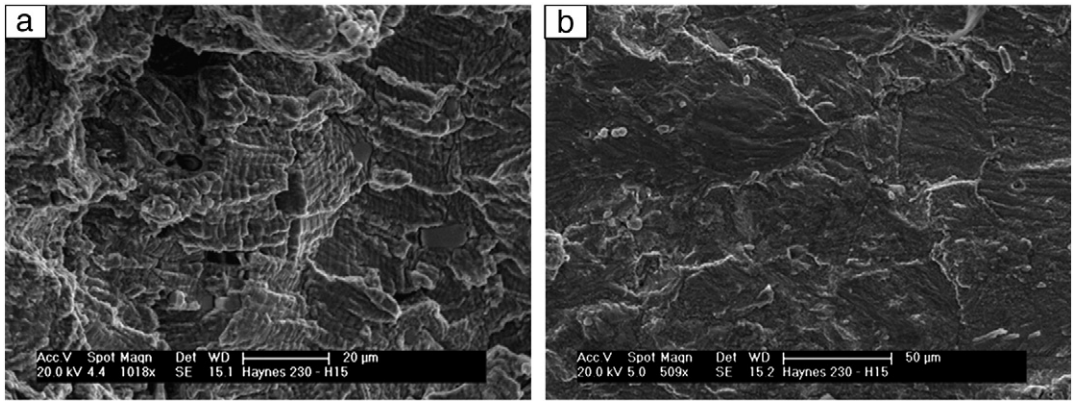

Fig. 9 – a) A high magnification SEM micrograph showing the fatigue striations on the 900 °C specimen. b) The post-fracture surface of the 900 °C specimen showing a low level of oxidation and a smooth surface indicative of intragranular fatigue crack growth.

along the stacking fault is believed to be of the M_6C type and has far less interaction with dislocations than the $M_{23}C_6$ carbides.

4. Discussion

4.1. *Crack Closure Effects*

As reported in Section 3.2, crack closure was present for both cases. Crack closure phenomena have been extensively studied beginning with Christensen who discovered roughness induced crack closure in 1963 [30]. Due to the pure mode I loading on the specimens tested in this study, roughness induced crack closure was concluded not to be the main crack closure phenomenon. Mode II loading is typically necessary to see roughness effects. By observing the crack faces on the failed specimens, very little deviations and asperities were seen supporting the previous conclusion. Thus, other forms of crack closure had to be considered.

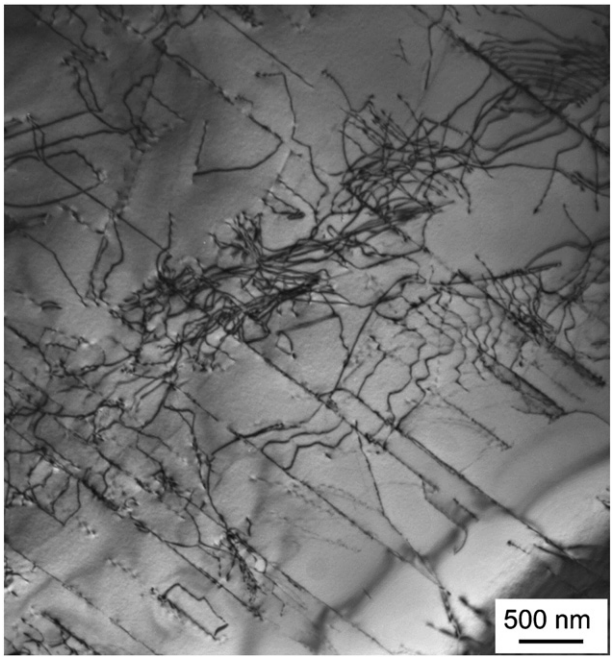

Fig. 10 – Planar slip in the Haynes 230 material.

By first taking into account the RT and HT cases together, plasticity induced crack closure was the most likely form of crack closure present in this study. Elber first discovered this phenomenon and found that the residual plasticity stretching from the crack tip across the entire crack face provided a shielding mechanism from the remote loading [31,32]. The DIC strain fields showed residual plasticity behind the crack tip and in shear bands extending from the crack tip. From this result it can be gleaned that plasticity induced crack closure is present and is the dominating form of crack closure. Previously, studies have concluded that load ratio, R, effects are minimized when considering the effective stress intensity factor range [33]. Other studies have looked at the crystallography of single crystals and found that the effective stress intensity factor range can also be used to eliminate scatter in fatigue crack growth data [7]. The usefulness of taking into account crack closure is evident for removing the dependence on the loading conditions, but does not account for the differences in RT and HT fatigue crack growth rates seen in this investigation.

At high temperatures, the propagation rate of cracks can be several orders of magnitude higher than that at room temperature. This has also been shown in previous fatigue crack growth studies of Haynes 230 [34,35]. Under these conditions, the crack tip might experience creep and environmental attack. Oxidation and hold times have been shown to increase the crack growth rate of Haynes 230 at highly elevated temperatures [26,27,35]. In order to determine the effects of these high temperature phenomena, oxide-induced crack closure must be considered in the HT case.

Although this nickel-based superalloy has excellent oxidation resistance and a high frequency was chosen in an effort to minimize environmental effects, the freshly exposed material due to the crack growth is still oxidized. Investigations were performed in the 1980s to determine the effect that oxides

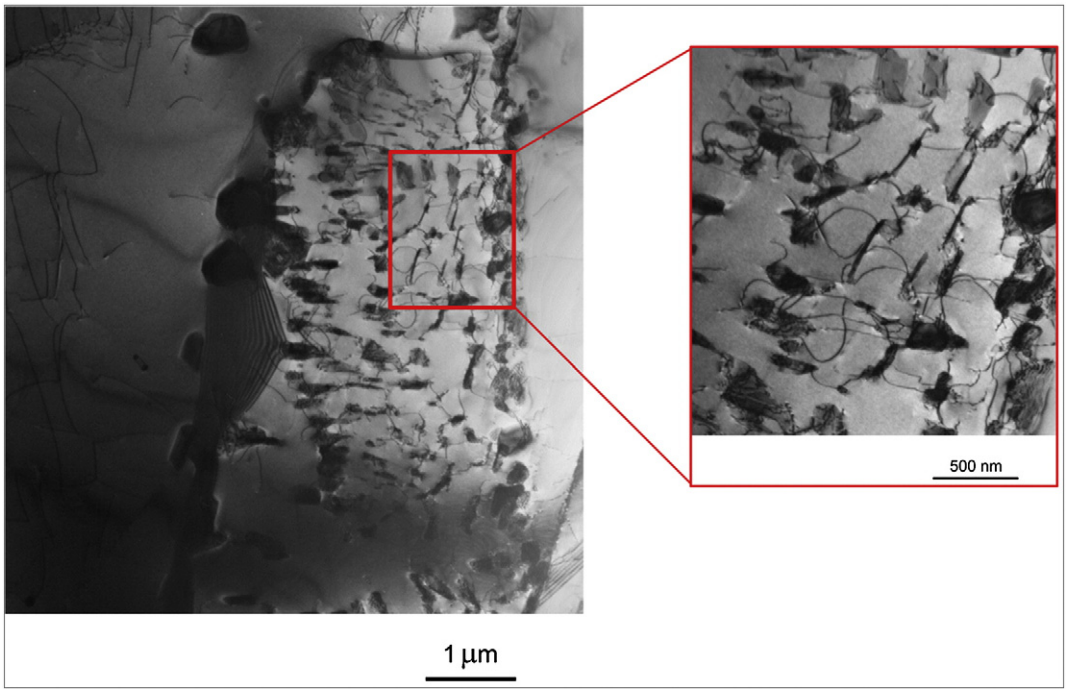

Fig. 11 – A TEM micrograph showing the heterogeneity in Haynes 230. A stacking fault separates areas of low carbide density and high carbide density. The cutout shows a dense area of carbide-dislocation interactions.

have on fatigue crack growth in steels [36], copper [37], and nickel-based superalloys [38]. Ritchie, Suresh, and Moss commented that the oxide films forming at the crack tip and any fretting of this film due to the roughness induced crack closure will increase the closure and decrease ΔK [39]. Although this information sheds light onto the role of crack closure on the fatigue crack growth in this study, both specimens in this current study show the same level of crack closure of about 30%. Also, an important finding in the literature is that oxide thickness needs to exceed or equal the crack tip opening displacement (CTOD) to have an effect. This is not the case for the crack growth condition studied here. Therefore, crack closure provides no explanation for the much faster crack growth rates in the HT case.

4.2. *Slip Irreversibility*

As discussed in the Introduction, the crack tip is the other area of interest for understanding the mechanics of fatigue crack growth. Dislocation interactions with the microstructure features, whether these are grain/twin boundaries or defects, control the slip irreversibility during a fatigue cycle. This occurs when dislocations interact with boundaries and a residual dislocation is left within that boundary [40]. Certain types of boundaries can play a significant role in increasing the resistance to fatigue crack growth and have been the focus of "grain boundary engineering". These boundaries are typically described as low sigma numbered, as defined in terms of coincidence site lattice theory [41]. Of particular interest have been annealing twins or $\Sigma 3$ boundaries and studies have shown that a greater number of $\Sigma 3$ boundaries leads to increased fatigue crack growth resistance. The twin boundary acts as a barrier to slip leading to a dislocation pile-up and a stress field that prevents dislocations from being emitted from the crack tip [20]. The microstructure of the Haynes 230 used in this study was described in Section 2.1 and the very high amount of $\Sigma 3$ boundaries found in this nickel-based alloy contributes to its good fatigue crack growth resistance (Paris exponent of $m \sim 2$).

As seen in Fig. 10, Haynes 230 demonstrated planar slip. Planar slip is commonly associated with solid solution hardened nickel-based superalloys and is encouraged by the inclusion of tungsten which reduces the stacking fault energy. This characteristic of the alloy leads to decreased slip irreversibility which reduces the fatigue crack growth rate [42]. Mughrabi quantified the cyclic slip irreversibility as the ratio between the irreversible plastic shear slip and the total cumulative plastic shear slip [43]. This idea was the basis of the measurements made in Section 3.3. The results concurred with Mughrabi and showed increasing fatigue crack growth rates with increasing slip irreversibility.

A relationship exists between the slip irreversibilites, crack growth rates, and temperature as the irreversibilities and growth rates were an order of magnitude higher for the HT case compared to the RT case. Since the cyclic frequency was high enough to minimize creep effects, the high temperature effects on dislocation motion must be elucidated. Increased temperature increases the cross-slip of screw dislocations and reduces the reversible slip since they will no longer return on that glide plane [43]. Dislocation climb, vacancies, and the annihilation of dislocations all prevent the return of dislocations to the crack tip [44,45]. The addition of this high temperature plastic flow has a direct influence on the slip irreversibility and therefore directly impacts the fatigue crack growth rate. It has also been well established that subgrain

formation occurs at high temperatures since the first observations in 1935 [46]. Since subgrains have a slightly different orientation compared to the surrounding material, the slip planes will be realigned. This creates a discontinuity of slip [47]. Previous research has indicated that the presence of barriers which prohibit the reverse of slip during the unloading portion of a fatigue cycle will increase the amount of slip irreversibility [20]. Due to the increased amount of subgrains present at HT compared to RT, it is expected that a much higher amount of slip irreversibility would be found. These effects are evident by the much higher fatigue crack growth rate of the HT specimen compared to the RT specimen as shown in Fig. 5. This study provided quantitative, experimental evidence that slip irreversibility is able to describe the fatigue crack growth rate differences between experiments with differing temperatures.

5. Conclusions

The fatigue crack growth of Haynes 230 was studied at room temperature (RT) and high temperature (HT). Analysis focused on the significance of any crack closure and the crack tip slip irreversibility and how these two phenomena are related to the crack growth rates.

1. The material showed good fatigue crack growth resistance both in the RT and HT tests ($m \sim 2$) although the HT fatigue crack grew at an appreciably faster rate. The role of microstructure is manifested through the irreversibility of slip at the crack tip.
2. Crack closure levels of approximately 30% of the load were determined at both test temperatures. Plasticity-induced crack closure was the main form of crack closure present and oxide-induced crack closure was not a significant factor in the HT case.
3. Slip irreversibility was quantitatively measured as the difference in accumulated strain per cycle at the crack tip, and it was over an order of magnitude higher in the HT case compared to the RT case.
4. Dislocations emitted at the crack tip were influenced by high temperature effects as reflected in the slip irreversibility measurements. Quantitative measurements of slip irreversibility were found to be an accurate method to distinguish the differences between the differences of crack growth rates at HT and RT.

Acknowledgements

The research was supported by the US Department of Energy Nuclear Energy University Program (NEUP) under grant DOE-INL-00091210. The authors acknowledge the help of Dr. T. Niendorf with the EBSD measurements.

Appendix. Least Squares Anisotropic Regression

The least squares anisotropic regression used during this study utilized the vertical DIC displacements to find the effective stress intensity factors. This is an ideal analysis technique since it is directly based on the experimental data. Crack closure effects were inherently included in the analysis since the crack opening displacements were influenced by any crack closure phenomena present. Only the vertical displacements were used since the crack only opened in the tensile , mode I manner.

The vertical displacements as a function of the mode I stress intensity factor, K_I, T-stress, and rigid body motion for plane stress are

$$v \quad \frac{K_I}{} \quad \frac{r}{2} \sin \quad \frac{}{2} \quad \frac{1}{2} \quad \frac{3}{1} \qquad 1 \quad \cos \quad \frac{}{2} \qquad \frac{1}{2} \quad \frac{}{1} \quad Tr \sin$$

$$Ar \cos \qquad B \qquad \text{A:1}$$

where A is the rigid body rotation coefficient, B is the rigid body translation coefficient, T is the T-stress term, r is the distance from the crack tip, is the angle from the crack line ahead of the tip, v is Poisson's ratio, and is the shear modulus. Thousands of vertical displacements, v, for each level of the load were known from the DIC correlations at their specific locations given by r and . The shear modulus and Poisson's ratio were obtained for the material at each temperature. A least squares regression was then employed to find the four unknowns (K_I, T, A, and B). Details of a similar least squares approach are given in McNeill *et al.* [48].

REFERENCES

[1] INL. Next generation nuclear plant materials research and development program plan, INL/EXT-06-11701; 2006.
[2] McEvily Jr AJ. On Crack Closure in Fatigue Crack Growth, Mechanics of Fatigue Crack Closure, ASTM STP - 982; 1988. p. 35-43.
[3] Schijve J. Fatigue crack closure: observations and technical significance, ASTM STP - 982; 1988. p. 5–34.
[4] Carroll J, Efstathiou C, Lambros J, Sehitoglu H, Hauber B, Spottswood S, et al. Investigation of fatigue crack closure using multiscale image correlation experiments. Eng Fract Mech 2009;76:2384.
[5] Riddell WT, Piascik RS, Sutton MA, Zhao W, McNeill SR, Helm JD. Determining fatigue crack opening loads from near-crack-tip displacement measurements, ASTM STP - 1343; 1999. p. 157.
[6] Sutton MA, Zhao W, McNeill SR, Helm JD, Piascik RS, Riddell WT. Local crack closure measurements: Development of a measurement system using computer vision and a far-field microscope, ASTM STP - 1343; 1999. p. 145.
[7] Sangid MD, Pataky GJ, Sehitoglu H, Hamilton RF, Maier HJ. High resolution analysis of opening and sliding in fatigue crack growth. Int J Fatigue 2011;37:134.
[8] Tomkins B. Fatigue crack propagation-an analysis. Phil Mag 1968;18:1041.
[9] McClintock FA. On the plasticity of the growth of fatigue cracks. Fract Solids 1963:65–102.
[10] Rice JR. The mechanics of crack tip deformation and extension by fatigue, Fatigue Crack Propagation, ASTM STP - 415; 1967.
[11] Brown MW, Miller KJ. Mode I Fatigue Crack Growth under Biaxial Stress at Room and Elevated Temperature, ASTM STP - 853; 1985. p. 135.

[12] Gao H, Alagok N, Brown MW, Miller KJ. Growth of Fatigue Cracks under Combined Mode I and Mode II Loads, ASTM STP - 853; 1985. p. 184.
[13] McClung RC, Sehitoglu H. On the finite element analysis of fatigue crack closure–2. Numerical results. Eng Fract Mech 1989;33:253.
[14] McEvily Jr AJ, Boettner RG. On fatigue crack propagation in F.C.C. metals. Acta Metall 1963;11:725.
[15] Forsyth PJE. Fatigue damage and crack growth in aluminium alloys. Acta Metall 1963;11:703.
[16] Fong C, Tromans D. High frequency stage I corrosion fatigue of austenitic stainless steel (316L). Metall Mater Trans A 1988;19:2753.
[17] Pippan R. Dislocation emission and fatigue crack growth threshold. Acta Metall Mater 1991;39:255.
[18] Pippan R. The condition for the cyclic plastic deformation of the crack tip: the influence of dislocation obstacles. Int J Fract 1992;58:305.
[19] Wu X, Koul A, Krausz A. A transgranular fatigue crack growth model based on restricted slip reversibility. Metall Mater Trans A 1993;24:1373.
[20] Sangid MD, Pataky GJ, Sehitoglu H, Rateick RG, Niendorf T, Maier HJ. Superior fatigue crack growth resistance, irreversibility, and fatigue crack growth microstructure relationship of nanocrystalline alloys. Acta Mater 2011;59: 7340.
[21] Sutton M, Orteu J-J, Schreier H. Image Correlation for Shape Motion and Deformation Measurements: Basic Concepts, Theory and Applications. Spring Media; 2009.
[22] Sutton MA, Wolters WJ, Peters WH, Ranson WF, McNeill SR. Determination of displacements using an improved digital correlation method. Image Vision Comput 1983;1:133.
[23] Tada H, Paris PC, Irwin GR. The stress analysis of cracks handbook. Hellertown, Pa: Del Research Corp.; 1973.
[24] Suresh S. Fatigue of materials. Cambridge, UK: Cambridge University Press; 1991.
[25] Anderson TL. Fracture Mechanics: Fundamentals and Applications. second ed.Boca Raton: CRC Press; 1994.
[26] Kim D, Jang C, Ryu W. Oxidation Characteristics and Oxide Layer Evolution of Alloy 617 and Haynes 230 at 900 °C and 1100 °C. Oxid Met 2009;71:271.
[27] Kun M, Gianfranco L, Hsiao-Ming T, Xiang C, James FS. High Temperature Aging and Corrosion Study on Alloy 617 and Alloy 230. J Eng Gas Turbines Power 2011;133:052908.
[28] Gerold V, Karnthaler HP. On the origin of planar slip in f.c.c. alloys. Acta Metall 1989;37:2177.
[29] Gell M, Leverant GR. Mechanisms of High-Temperature Fatigue, Fatigue at Elevated Temperatures ASTM STP - 520; 1973. p. 37-67.
[30] Christensen RH. Fatigue crack growth affected by metal fragments wedged between opening-closing crack surfaces. Appl Mater Res 1963;2:207.
[31] Elber W. Fatigue crack closure under cyclic tension. Eng Fract Mech 1970;2:37.
[32] Elber W. The Significance of Fatigue Crack Closure, ASTM STP - 486; 1971. p. 230.
[33] Staal HU, Elen JD. Crack closure and influence of cycle ratio R on fatigue crack growth in type 304 stainless steel at room temperature. Eng Fract Mech 1979;11:275.
[34] Lee S, Lu Y, Liaw P, Choo H, Thompson S, Blust J, et al. High-temperature tensile-hold crack-growth behavior of Hastelloy X alloy compared to HAYNES 188 and HAYNES 230 alloys. Mech Time-Depend Mater 2008;12:31.
[35] Lu YL, Chen LJ, Liaw PK, Wang GY, Brooks CR, Thompson SA, et al. Effects of temperature and hold time on creep-fatigue crack-growth behavior of HAYNES 230 alloy. Mater Sci Eng A 2006;429:1.
[36] Suresh S, Zamiski G, Ritchie D. Oxide-Induced Crack Closure: An Explanation for Near-Threshold Corrosion Fatigue Crack Growth Behavior. Metall Mater Trans A 1981;12:1435.
[37] Liaw PK, Leax TR, Williams RS, Peck MG. Influence of oxide-induced crack closure on near-threshold fatigue crack growth behavior. Acta Metall 1982;30:2071.
[38] King JE. Surface damage and near-threshold fatigue crack growth in a Ni-base superalloy in vacuum. Fatigue Fract Eng Mater Struct 1982;5:177.
[39] Ritchie RO, Suresh S, Moss CM. Near-Threshold Fatigue Crack Growth in 2 1/4 Cr-1Mo Pressure Vessel Steel in Air and Hydrogen. J Eng Mater Technol 1980;102:293.
[40] Ezaz T, Sangid MD, Sehitoglu H. Energy barriers associated with slip-twin interactions. Phil Mag 2007;91:1464.
[41] Gao Y, Ritchie R, Kumar M, Nalla R. High-cycle fatigue of nickel-based superalloy ME3 at ambient and elevated temperatures: Role of grain-boundary engineering. Metall Mater Trans A 2005;36:3325.
[42] Mott NF. A theory of the origin of fatigue cracks. Acta Metall 1958;6:195.
[43] Mughrabi H. Cyclic Slip Irreversibilities and the Evolution of Fatigue Damage. Metall Mater Trans A 2009;40:1257.
[44] Pineau A, Antolovich SD. High temperature fatigue of nickel-base superalloys - A review with special emphasis on deformation modes and oxidation. Eng Fail Anal 2009;16: 2668.
[45] Ellyin F. Fatigue Damage, Crack Growth and Life Prediction. Springer; 1996.
[46] Jenkins CHM, Mellor GA. Investigation of behaviour of metals under deformation at high temperatures – 1. J Iron Steel Inst 1935;132:179.
[47] Manson S. Fatigue: A complex subject—Some simple approximations. Exp Mech 1965;5:193.
[48] McNeill SR, Peters WH, Sutton MA. Estimation of stress intensity factor by digital image correlation. Eng Fract Mech 1987;28:101.